Search for pair-production of new heavy colored particles decaying to pairs of jets in $p\bar{p}$ collisions at $\sqrt{s} = 1.96$ TeV

We present a search for the pair-production of a heavy colored particle Y which decays to a pair of quarks or gluons, leading to a final state with four hadronic jets. We consider both non-resonant production via an intermediate gluon as well as resonant production via a heavy intermediate colored particle X. In data collected by the CDFII experiment in $p\bar{p}$ collisions at $\sqrt{s} = 1.96$ TeV corresponding to integrated luminosity of 6.6 fb^{-1}, we find the data to be consistent with standard model predictions. We report limits on $\sigma(p\bar{p} \to YY \to jjjj)$ versus m_Y and $\sigma(p\bar{p} \to X \to YY \to jjjj)$ versus m_X and m_Y. In the context of non-resonant coloron C production, we exclude m_C between 50 and 125 GeV/c^2; in an R-parity-violating stop quark $\tilde{t}$ hypothesis we exclude $m_{\tilde{t}}$ between 50 and 100 GeV/c^2. In the context of hyperpions produced via an axi-gluon resonance A, we exclude m_A between 100 and 400 GeV/c^2 for coupling values preferred by the anomaly in the CDF top-quark forward-backward asymmetry.

PACS numbers:

One of the few hints of new physics at the TeV scale is the CDF top-quark forward-backward asymmetry A_{fb} measurement [1–3]. Many theoretical models have been proposed to explain this result, most with specific predictions of excesses which would confirm their hypotheses. However, nearly all have been excluded, mostly due to the lack of excesses of same-sign top-quark pair production [4, 5], or top+jet resonances [6–8]. One of the last remaining viable models is the production of top-quark pairs via a light axi-gluon which interferes with standard model (SM) $t\bar{t}$ production to produce the observed asymmetry. The axi-gluon would be visible in its alternate decay mode to low-mass colored particles, each of which decay to a pair of jets [9] giving a four-jet final state. This final state is of broad interest, as other models predict pair-production of colorons decaying to jet pairs with no intermediate resonance [10, 11] and R-parity-violating supersymmetric theories predict pair-production of light stop quarks which each decay to pairs of light quarks.

The mass of the axi-gluon or its colored decay products are not predicted, but must be fairly light to explain the A_{fb} measurement [12]. The LHC experiments have excellent sensitivity at high mass due to the large center-of-mass energy, but difficulties at low mass due to high interaction rates. The ATLAS experiment ruled out masses between 100 and 150 GeV/c^2 [13] but could not probe lower masses due to trigger rates. There are no limits below 100 GeV/c^2 for non-resonant pair-production of di-jet resonances, and no limits on resonant production.

This Letter reports a search for both non-resonant and resonant production of pairs of colored particles, each of which decay to a pair of jets. Rather than probing a specific theory, we construct a simplified model with the minimal particle content. In the non-resonant case, we consider production $p\bar{p} \to YY \to jj\ jj$, with a single parameter m_Y. In the resonant case, $p\bar{p} \to X \to YY \to jj\ jj$, we explore two parameters, m_X and m_Y. See Figure 1.

We analyze a sample of events corresponding to an integrated luminosity of 6.6±0.5 fb^{-1} recorded by the CDF II detector [14], a general purpose detector designed to study $p\bar{p}$ collisions at $\sqrt{s} = 1.96$ TeV produced by the Fermilab Tevatron collider. CDF's tracking system consists of a silicon microstrip tracker and a drift chamber that are immersed in a 1.4 T axial magnetic field [15]. Electromagnetic and hadronic calorimeters surrounding the tracking system measure particle energies, with muon detection provided by an additional system of drift chambers located outside the calorimeters.

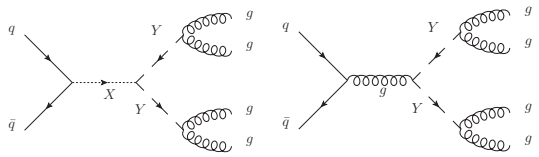

FIG. 1: Diagrams for resonant (left, via X) and non-resonant (right) pair-production of Y, with subsequent decays to pairs of gluons.

We reconstruct jets in the calorimeter using the JETCLU [16] algorithm with a clustering radius of 0.4 in $\eta - \phi$ space, and calibrated using the techniques outlined in Ref. [17]. Events are selected online (triggered) by the requirement of three jets, each with $E_T > 20$ GeV and with $\Sigma E_T > 130$ GeV [18]. After trigger selection, events are retained if at least four jets are found with $E_T > 15$ GeV and $|\eta| < 2.4$.

We model the production of resonant and non-resonant production with MADGRAPH5 [19] version 1.4.8.4 and the CTEQ6L [20] parton distribution function (PDF). Additional radiation, hadronization and showering are described by PYTHIA [21] version 6.420. The detector response for all simulated samples is modeled by the GEANT-based CDF II detector simulation [22].

The trigger and selection have an efficiency up to 90% if ΣE_T is well above the 130 GeV trigger threshold. Below that, the efficiency drops rapidly, see Fig. 2. In the

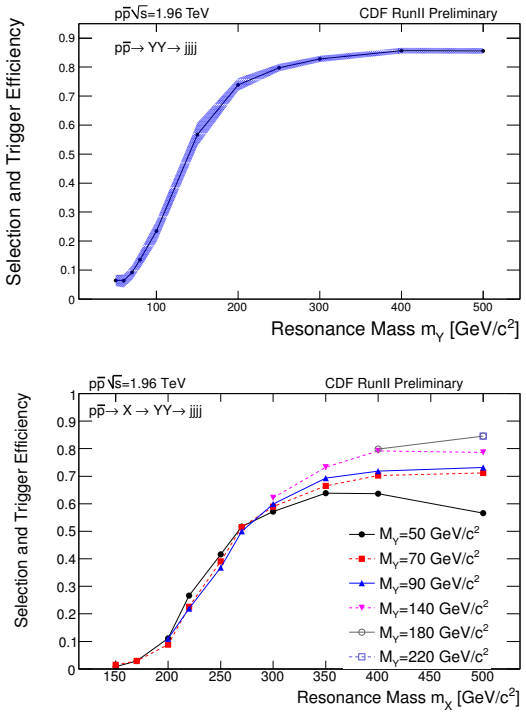

FIG. 2: Overall efficiency, including trigger and selection requirements. Top, efficiency for several simulated non-resonant $YY \to jjjj$ samples with varying m_Y. The shaded band shows the uncertainty; similar uncertainties, not shown, apply to the bottom pane. Bottom, efficiency for several simulated resonant $X \to YY \to jjjj$ samples with varying m_X and m_Y. The turn-on curve is determined largely by the trigger requirement that $\Sigma E_T > 130$ GeV.

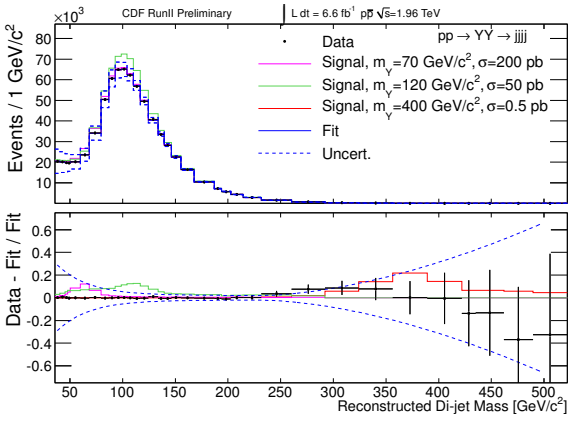

FIG. 3: Reconstructed mean di-jet mass in events with four jets. Top pane shows the events, with a parametric fit and several signal hypotheses overlaid. Bottom pane shows the relative difference between the observed data and the fit in each bin.

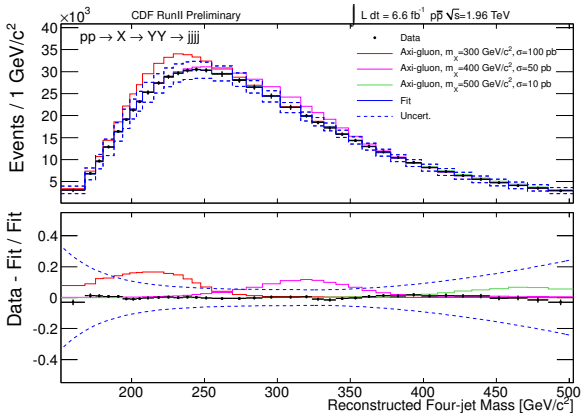

FIG. 4: Reconstructed mean four-jet mass in events with four jets. Top pane shows the events, with a parametric fit and several signal hypotheses overlaid. Bottom pane shows the relative difference between the observed data and the fit in each bin.

non-resonant-production model, the ΣE_T is strongly correlated with m_Y. In the resonant-production model it is correlated with m_X; additionally if $m_X - m_Y$ is large, the p_T of the resulting Y is large, which leads to a small opening angle of its decay products and a loss of efficiency due to merged jets.

To reconstruct the di-jet resonance, we consider the four leading jets and evaluate the invariant mass of each of the di-jet pairs in the three permutations, choosing the permutation with the smallest mass difference between the pairs. As the pair masses are correlated, we take the mean of the two pair masses as the estimate of the di-jet resonance mass. To reduce background levels, we require that the relative mass difference is less than 50%, and that the production angle θ^* of the di-jet resonance in the center-of-mass frame satisfies $\cos(\theta)^* < 0.9$. In the resonant production analysis, we calculate the four-jet invariant mass. No specific m_Y-dependent selections are made; the requirement that the relative di-jet mass difference be small ensures compatability with the $X \to YY$ hypothesis.

The dominant background is multi-jet production. We model this background contribution using a parametric function which is fit to the reconstructed mass spectrum of the observed data. The function is a piecewise combination of a third-order polynomial to describe the turn-on region, a third-order polynomial to describe the peak region and a double-exponential of the form $f(m) = a_1 e^{-(m-a_2)^{a_3}/a_4}$ to describe the falling spectrum. For the di-jet mass, the ranges used are $[35, 82.5]$, $[82.5, 140]$, and $[140, 700]$ GeV/c^2; for the four-jet mass, the ranges used are $[115, 185]$, $[185, 330]$, and $[330, 800]$ GeV/c^2. The functional form was chosen based on its ability to accurately describe the mass spectra of simulated multi-jet events generated by ALPGEN [23] version 2.10.

The dominant source of systematic uncertainty is due to the multi-jet background model. The parametric functional form was chosen to be flexible enough to describe

the multi-jet mass spectrum, but rigid enough to avoid accurately describing a spectrum which includes a narrow resonance, so that in the presence of a real signal a signal-plus-background hypothesis would be preferred. The functional form is an approximation, which even in the absence of a narrow feature may deviate from the observed spectrum. We estimate the impact of these potential deviations by measuring their magnitude in two control samples in which the signal is depleted. The first requires a large relative di-jet mass difference, greater than 50%, and the second requires $\cos(\theta)^* > 0.9$. The observed relative deviations are then applied to the observed spectrum in the signal region to estimate the magnitude of spurious deviations due to the imperfect functional form.

An additional uncertainty is due to our knowledge of the trigger efficiency [24] of the simulated signal samples, varying from 20% relative at $\Sigma E_T = 120$ GeV to 10% above $\Sigma E_T = 200$ GeV. Uncertainties in the calibration of the jet energy and resolution modeling also contribute to uncertainties in the efficiency and reconstructed mass spectrum of the signal samples, though these are small relative to the fitting and trigger uncertainties.

In the non-resonant analysis, for each Y mass hypothesis, we fit the most likely value of the Y pair-production cross section (σ_{YY}) by performing a binned maximum-likelihood fit of the di-jet mass distribution, allowing for systematic and statistical fluctuations via template morphing [25]. The likelihood is binned in di-jet mass and takes the form of

$$L(\sigma_{YY}) = \prod_{\text{bin } i} f^i_{\text{bg}}(\vec{a}) + \sigma_{YY} \times \mathcal{L} \times \epsilon \times f^i_{\text{sig}}$$

where $f_{\text{bg}}(\vec{a})$ is the parametric function with nuisance parameters $\vec{a}$ defined above to describe the background spectrum, f_{sig} is a normalized template of the expected shape of the signal built from simulated events, and $\mathcal{L} \times \epsilon$ is the product of the integrated luminosity and efficiency. No evidence is found for the presence of pair-production of di-jet resonances so we set upper limits on Y pair-production at 95% confidence level. Limits are calculated by performing hypothetical simulated experiments with the signal injected at a range of cross sections without profiling the systematic uncertainties; these experiments are used with the CLs method [26] to obtain the limits. The observed limits are consistent with expectation for the background-only hypothesis. The resonant analysis is very similar, but scans the X mass hypothesis, fitting the four-jet mass distribution for the most likely value of X production cross section, σ_X.

In the non-resonant case, this analysis sets the first limits on coloron or stop-quark pair production with masses below 100 GeV/c^2, see Table I and the top of Fig. 5. The uncertainty on the theoretical cross-section prediction is taken from an alternative PDF, MSTW2008LO [27], as well as a variation of the renormalization and factor-

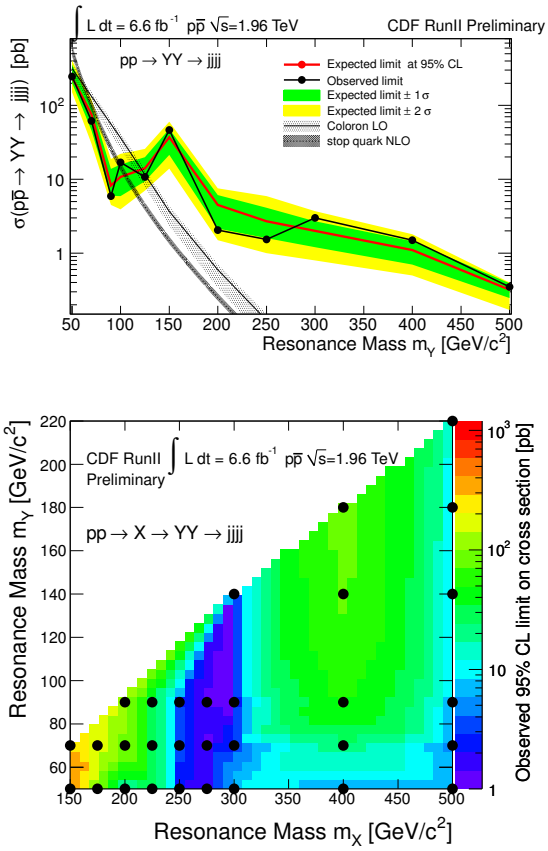

FIG. 5: Upper limits at 95% CL. Top, limits on $\sigma(p\bar{p} \to YY \to jjjj)$ versus m_Y in the non-resonant analysis. Two signal hypotheses are shown, see text for details. Bottom, limits on $\sigma(p\bar{p} \to X \to YY \to jjjj)$ versus m_X and m_Y. Circles indicate the grid of simulated samples where limits are evaluated; intervening values are interpolated.

TABLE I: Observed and expected 95% CL upper limits on $\sigma(p\bar{p} \to YY \to jjjj)$ for several values of m_Y. Also shown are theoretical predictions for coloron pair production [10, 11] or stop-quark pair production with R-parity violating decay $\tilde{t} \to qq'$ [28].

CDF RunII Preliminary $\int \mathcal{L}dt = 6.6$ fb^{-1}				
Mass	Expected	Observed	Coloron	stop quarks
(GeV/c^2)	(pb)	(pb)	(pb)	(pb)
50	239.5	246.8	320	570
70	75.3	61.9	180	100
90	8.2	5.9	62	26
100	10.8	16.9	37	15
125	14.0	10.8	11	4.4
150	37.2	46.4	3.7	1.5
200	4.5	2.0	0.60	0.25
250	2.7	1.5	0.11	$5.4 \cdot 10^{-2}$
300	2.0	3.0	$2.9 \cdot 10^{-2}$	$1.3 \cdot 10^{-2}$
400	1.1	1.5	$1.7 \cdot 10^{-3}$	$7.2 \cdot 10^{-4}$
500	0.3	0.3	$8.5 \cdot 19^{-5}$	$3.6 \cdot 10^{-5}$

TABLE II: Observed and expected 95% CL upper limits on $\sigma(p\bar{p} \to X \to YY \to jjjj)$ for several values of m_Y and m_X. Also shown are theoretical predictions for axi-gluon production assuming coupling to quarks of $C_q = 0.4$ [9, 12].

CDF RunII Preliminary $\int \mathcal{L}dt = 6.6$ fb^{-1}				
m_X (GeV/c^2)	m_Y (GeV/c^2)	Expected (pb)	Observed (pb)	Axi-gluon (pb)
150	50	641.2	431.1	5600
	70	209.6	270.6	
175	50	66.8	78.9	3500
	70	111.5	163.9	
200	50	13.8	9.5	2200
	70	30.4	91.5	
	90	17.8	100.4	
225	50	18.0	26.0	1750
	70	20.7	25.0	
	90	20.9	25.3	
250	50	6.2	2.0	1000
	70	4.0	3.6	
	90	5.1	2.8	
275	50	6.5	1.2	850
	70	7.7	1.3	
	90	9.7	1.4	
300	50	5.0	7.1	540
	70	2.4	2.6	
	90	1.7	1.0	
	140	1.8	1.2	
400	50	15.5	6.8	170
	70	15.0	20.2	
	90	30.6	52.8	
	140	41.0	74.6	
	180	46.9	79.1	
500	50	20.7	6.8	60
	70	15.9	4.7	
	90	17.7	5.9	
	140	25.2	7.0	
	180	26.7	8.0	
	220	29.7	9.3	

ization scales by a factor of two in each direction. In the resonant case, this analysis excludes axi-gluon production in the case of coupling to quarks $C_q = 0.4$ (see Table II and the bottom of Fig. 5) which is close to the value required to explain the top A_{fb} result [12]. To be consistent with our limits, the couplings would have to be lower by an order of magnitude; maintaining consistency with the top A_{fb} result would require different couplings to light-quarks and heavy-quarks, with the heavy-quark coupling approaching the perturbative limit.

We thank Martin Schmaltz, Gustavo Tavares, Can Kilic, Bogdan Dobrescu, Dirk Zerwas and Felix Yu for useful suggestions and technical advice. We thank the Fermilab staff and the technical staffs of the participating institutions for their vital contributions. This work was supported by the U.S. Department of Energy and National Science Foundation; the Italian Istituto Nazionale di Fisica Nucleare; the Ministry of Education, Culture, Sports, Science and Technology of Japan; the Natural Sciences and Engineering Research Council of Canada; the National Science Council of the Republic of China; the Swiss National Science Foundation; the A.P. Sloan Foundation; the Bundesministerium für Bildung und Forschung, Germany; the Korean World Class University Program, the National Research Foundation of Korea; the Science and Technology Facilities Council and the Royal Society, UK; the Russian Foundation for Basic Research; the Ministerio de Ciencia e Innovación, and Programa Consolider-Ingenio 2010, Spain; the Slovak R&D Agency; the Academy of Finland; and the Australian Research Council (ARC).

[1] T. Aaltonen *et al.* [CDF Collaboration], Phys. Rev. Lett. **101**, 202001 (2008).
[2] V. M. Abazov *et al.* [D0 Collaboration], Phys. Rev. Lett. **100**, 142002 (2008).
[3] T. Aaltonen *et al.* [CDF Collaboration], Phys. Rev. D **83**, 112003 (2011).
[4] S. Chatrchyan et al. [CMS Collaboration], JHEP 1108, 005 (2011).
[5] G. Aad *et al.* [ATLAS Collaboration], JHEP **1204**, 069 (2012).
[6] CDF Collaboration, T. Aaltonen et al., Phys Rev. Lett. 108 211805 (2012).
[7] S. Chatrchyan *et al.* [CMS Collaboration], Phys. Lett. B **717**, 351 (2012).
[8] G. Aad *et al.* [ATLAS Collaboration], arXiv:1209.6593 (2012).
[9] G. Marques Tavares and M. Schmaltz, Phys. Rev. D **84**, 054008 (2011)
[10] Y. Bai and B. A. Dobrescu, JHEP **1107**, 100 (2011).
[11] C. Kilic, S. Schumann and M. Son, JHEP **0904**, 128 (2009).
[12] C. Gross, G. M. Tavares, C. Spethmann and M. Schmaltz, arXiv:1209.6375 [hep-ph] (2012).
[13] G. Aad *et al.* [ATLAS Collaboration], Eur. Phys. J. C **71**, 1828 (2011).
[14] T. Aaltonen *et al.* (CDF Collaboration), Phys. Rev. D **71**, 032001 (2005).
[15] C. S. Hill, Nucl. Instrum. Methods A **530**, 1 (2004).
[16] T. Aaltonen *et al.* (CDF Collaboration), Phys. Rev. D **45**, 001448 (1992).
[17] A. Bhatti *et al.*, Nucl. Instrum. Methods A **566**, 375 (2006).
[18] CDF uses a cylindrical coordinate system with the z axis along the proton beam axis. For a particle or a jet, pseudorapidity is $\eta \equiv -\ln(\tan(\theta/2))$, where θ is the polar angle relative to the proton beam direction, and ϕ is the azimuthal angle while transverse momentum $p_T = |p| \sin\theta$, and the transverse energy $E_T = E \sin\theta$.
[19] J. Alwall, P. Demin, S. de Visscher, R. Frederix, M. Herquet, F. Maltoni, T. Plehn, D. L. Rainwater, and T. Stelzer, J. High Energy Phys. 09 (2007) 028.
[20] J. Pumplin *et al.* (CTEQ Collaboration), J. High. Energy Phys. 07 (2002) 012.
[21] T. Sjostrand *et al.*, Comput. Phys. Commun. **238**, 135 (2001), version 6.422.
[22] E. Gerchtein and M. Paulini, arXiv:physics/0306031

(2003).
[23] M. L. Mangano, M. Moretti, F. Piccinini, R. Pittau and A. D. Polosa, J. High Energy Phys. 07 (2003) 001.
[24] T. Aaltonen *et al.* [CDF Collaboration], Phys. Rev. D **84**, 052010 (2011).
[25] A. Read, Nucl. Instrum. Methods A **425**, 357 (1999).
[26] A. Read, J. Phys. G: Nucl. Part. Phys. **28**, 2693 (2002); T. Junk, Nucl. Instrum. Methods A **434**, 425 (1999).
[27] A. D. Martin, W. J. Stirling, R. S. Thorne and G. Watt, Eur. Phys. J. C **63**, 189 (2009).
[28] W. Beenakker, M. Kramer, T. Plehn, M. Spira and P. M. Zerwas, Nucl. Phys. B **515**, 3 (1998).

ADDITIONAL PLOTS

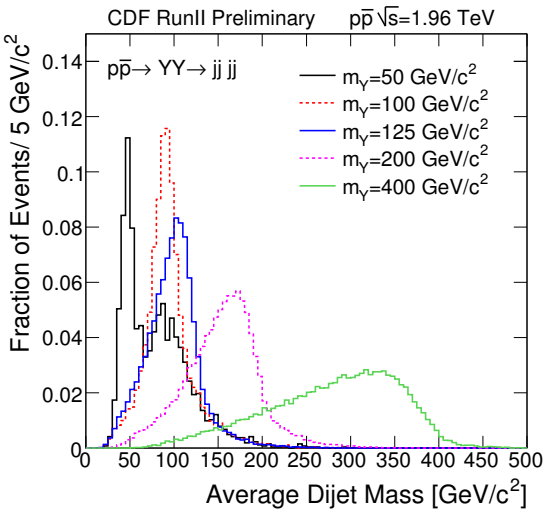

FIG. 6: Reconstructed average di-jet mass for several simulated non-resonant $YY \to jjjj$ samples with varying m_Y.

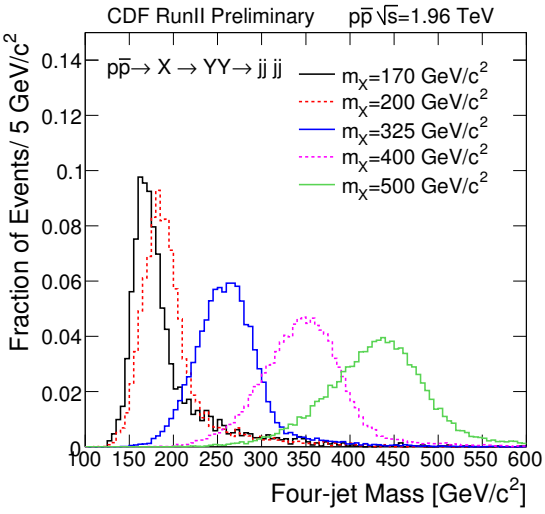

FIG. 7: Reconstructed four-jet mass for several simulated resonant $X \to YY \to jjjj$ samples with varying m_X for $m_Y = 50$ GeV/c^2.

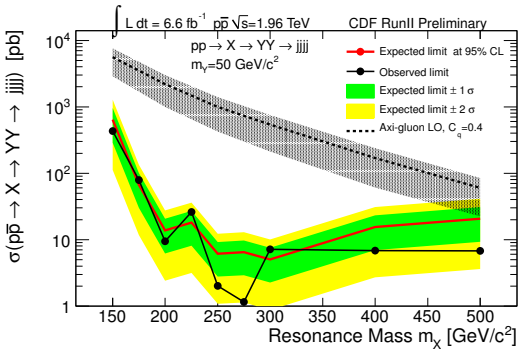

FIG. 8: Upper limits at 95% CL on $\sigma(p\bar{p} \to YY \to jjjj)$ versus m_X with $m_Y = 50$ GeV/c^2 in the resonant analysis. An axi-gluon signal hypothesis is shown, see text for details.